Journal of Power Sources 191 (2009) 678–683

Contents lists available at ScienceDirect

Journal of Power Sources

journal homepage: www.elsevier.com/locate/jpowsour

Construction of composite electrodes comprising manganese dioxide nanoparticles distributed in polyaniline–poly(4-styrene sulfonic acid-co-maleic acid) for electrochemical supercapacitor

Feng-Jiin Liu[a,*], Tsui-Fen Hsu[a], Chien-Hsin Yang[b]

[a] Department of Chemical Engineering, National United University, 1, Lien Da, Kung-Ching Li, Miao-Li 36003, Taiwan
[b] Department of Chemical and Materials Engineering, National University of Kaohsiung, Kaohsiung 811, Taiwan

ARTICLE INFO

Article history:
Received 18 August 2008
Received in revised form
26 December 2008
Accepted 13 February 2009
Available online 3 March 2009

Keywords:
Polyaniline
Poly(4-styrene sulfonic acid-co-maleic acid)
Manganese oxide
Supercapacitors
Specific capacitance

ABSTRACT

This work demonstrated a novel and simple route for preparing a composite comprising of manganese oxide (MnO_2) nanoparticles and polyaniline (PANI) doped poly(4-styrene sulfonic acid-co-maleic acid) (PSSMA) by "electrochemical doping-deposition". The PANI–PSSMA–MnO_2 composite was characterized by scanning electron microscopy (SEM)), X-ray diffraction (XRD) and X-ray photoelectron spectroscopy (XPS). SEM images revealed a uniform dispersion of MnO_2 nanoparticles in the porous structure of PANI–PSSMA structure. XRD measurements showed the distortion of the crystal structure of β-MnO_2 after deposition of MnO_2 in PANI–PSSMA structure. Thus, the XRD pattern of PANI was predominating. Cyclic voltammetry and chronopotentiometry were employed in 0.5 M Na_2SO_4 to evaluate the capacitor properties. The results showed a significant improvement in the specific capacitance of the composite electrode. The specific capacitance of PANI–PSSMA–MnO_2 (50.4 F g^{-1}) had improvement values of 172% compared to that of PANI (18.5 F g^{-1}). When only the MnO_2 mass was considered, the composite had a specific capacitance of 556 F g^{-1}.

1. Introduction

The electrochemical capacitors are being considered for various applications, not only coupled with batteries to provide peak power, but also to replace batteries for memory backup and for use in electric vehicles [1,2]. Electrochemical capacitors are categorized as electrical double-layer capacitors (EDLCs) and Faradic pseudocapacitors according to their fundamental charge–discharge mechanism. The former stores energy by charge separation at the electrode and electrolyte interface while the latter utilizes Faradic redox reactions.

Among the pseudocapacitor electrode materials, hydrous RuO_2 has been found to be most promising and has been extensively studied, and it exhibits high specific capacitance values ranges from 720 to 760 F g^{-1} [3,4]. However, the high cost and toxicity of RuO_2 limits its range of applications and have motivated the research into other transition metal oxides. Manganese oxide (MnO_2) is regarded as potentially useful material for pseudocapacitors because of not only their low cost but also their environment friendliness [5,6]. According to the literature, the specific capacitance of MnO_2 is between 150 and 250 F g^{-1} [7]. Prasad and Miura [8,9] have reported a capacitance of amorphous electrolytic MnO_2 (EMD) and MnO_2-based mixed oxides of between 400 and 621 F g^{-1}. Nevertheless, MnO_2-based pseudocapacitor electrodes are expected to have a higher capacitance (1370 F g^{-1}) [10].

Conducting polymers are a promising class of materials for use in electrochemical capacitors. The faster doping/dedoping mechanisms and ability to undergo both n- and p-doping are their main advantages. They have been utilized with carbon and transition metal oxides in pseudocapacitors [11,12,4]. Polyaniline (PANI) is one of the most promising conducting polymers with potential applications because of its easy synthesis, high stability, and good conductivity. Hence, when used as a substrate, PANI can improve the capacitive properties of another material that is deposited on it.

MnO_2 electrode materials for pseudocapacitor application have been prepared by various synthetic methods, including the sol–gel and solution-based chemical routes [13–15], electrochemical deposition [16,17], and sputtering followed by electrochemical oxidation [18]. Electrochemical deposition methods have been adopted extensively to disperse MnO_2 in polymer matrices [19,20]. Compared with other methods, such as sol–gel, solution-based chemical oxidation, and sputtering, electrodeposition has proven to be the least expensive and is highly productive and readily adoptable. Based on the potential-pH diagram of Mn [21], the deposition of MnO_2 from Mn^{2+} occurs at potentials of approximately 0.78 V

* Corresponding author. Tel.: +886 37 381572; fax: +886 37 332397.
E-mail address: liu@nuu.edu.tw (F.-J. Liu).

0378-7753/$ – see front matter © 2009 Elsevier B.V. All rights reserved.
doi:10.1016/j.jpowsour.2009.02.046

(vs. Ag/AgCl) at pH ≥ 4.0. One of the most important problems of employing PANI as matrix for depositing MnO_2 is the lack of electroactivity when the pH increases over 4.0. This investigation develops another strategy for extending the electroactivity of PANI and simultaneously depositing MnO_2 in the PANI matrix. In the work, "electrochemical doping" method is adopted to induce the SO_3H and COOH groups (poly(4-styrene sulfonic acid-co-maleic acid), sodium salt, PSSMA) into PANI. $MnSO_4$ was dissolved in PSSMA solution. Mn^{2+} ions were expected to interact with the excess SO_3^- and COO^- by electrostatic attractive force. Therefore, the electrochemical doping of PANI with PSSMA accompanied the embedding of MnO_2 in PANI–PSSMA. PANI–PSSMA behaves as an effective probe for depositing MnO_2 and increased the density of MnO_2 in the polymer film. This work elucidates the synthesis and characterization of PANI–PSSMA–MnO_2 composite film by the "electrochemical doping-deposition" method. The electrochemical properties of PANI–PSSMA–MnO_2 as a supercapacitor electrode material were extensively examined by means of cyclic voltammetry.

2. Experimental

2.1. Chemicals

Reagent-grade aniline (ANI) (Merck) was doubly distilled and the resulting colorless liquid was kept in the dark at 5 °C. Reagent-grade poly(4-styrene sulfonic acid-co-maleic acid) sodium salt (M_w = 75,000, Aldrich) was used without any further treatment. All solutions were prepared from doubly distilled water and $MnSO_4$ (Aldrich) and sulfuric sodium (Merck) were used as received.

2.2. Preparation of PANI–PSSMA–MnO_2

ANI was electrochemically polymerized by the potentiostatic method (0.8 V vs. Ag/AgCl) on indium tin oxide (ITO) electrodes as described elsewhere [22]. The mass of PANI deposited on ITO was 0.193 mg. The mass of PANI deposited on ITO was calculated from the following equation:

$$m = \frac{Q_{dep} \times M}{F \times Z}$$

where the mass (m) of PANI that was deposited on S.S. was calculated from the deposited charge (Q_{dep}). M is the molecular weight of ANI, F the Faradic constant and Z is the number of electron involved in the process.

The plating solutions, containing 0.25 M $MnSO_4$ and 0.1 M PSSMA at pH 6.5, were stirred on a hot plate during "electrochemical doping-deposition". Briefly, the "electrochemical doping-deposition" of a film was as follows; (a) emeraldine base form (EB) of PANI was dedoped by treating the PANI film with 1.0 M ammonium hydroxide until color of the film changed from green to blue. (b) SO_3^-/COO^- ions were doped in PANI by simply dipping PANI into PSSMA–$MnSO_4$ solution for 1–2 min. (c) "Electrochemical doping-deposition" was conducted to prepare PANI–PSSMA–MnO_2 by cycling the potential in the range of −0.2 to 1.0 V for 30 cycles with a scan rate of 50 mV s^{-1} and the cyclic voltammograms (CVs) were recorded during the synthesis. After MnO_2 particles were incorporated, the electrodes were rinsed in double distilled water for 5 min and then dried at 100 °C for 3 min.

2.3. Physical and electrochemical characterizations

The surface morphologies of the emeraldine base form of PANI and PANI–PSSMA–MnO_2 were observed using a scanning electron microscopy (Philips X1-40 FEG). X-ray diffraction (XRD) pattern of PANI–PSSMA–MnO_2 was obtained by exposing the sample to Siemens D5000-X-ray source with Cu Kα (1.542 Å). The spectra were scanned in the range 2θ = 10–90°. XPS measurements were made using ESCA 210 and Microlab 310 D (VG Scientific, Ltd., United Kingdom) spectrometers. XPS spectra were obtained with Mg Kα ($h\nu$ = 1256.6 eV) irradiation whose photon source was driven at 12 kV and at an emission current of 20 mA. The pressure in the base chamber of the spectrometer was kept at approximately 10^{-10} mbar during the measurements.

The electrochemical characterization of the catalyst was performed using PGSTAT20 electrochemical analyzer, AUTOLAB Electrochemical Instrument (The Netherlands). All the experiments were carried out in a three component cell in which an ITO coated glass plate (1 cm^2 area), Ag/AgCl (in 3 M KCl) and platinum wire were used as working, reference and counter electrodes, respectively. A Luggin capillary, whose tip was set at a distance of 1–2 mm from the surface of the working electrode, was adopted to minimize the potential drop across the electrolyte solutions.

3. Results and discussion

3.1. Characterization of PANI–PSSMA–MnO_2 composite

This work demonstrated a novel "electrochemical doping-deposition" route for simultaneously doping a PANI emeraldine base and embedding MnO_2. Fig. 1 shows the cyclic voltammograms that were recorded during the "electrochemical doping-deposition" of PSSMA and MnO_2 in the PANI film. In fact, PANI looses its electroactivity in neutral solution. In this work, the electrolyte contained PSSMA. The SO_3H and COOH groups pending on the PSSMA polymer chain can be ionized in neutral solution. The protons generated in the ionization process are supplied immediately to the electrochemical reaction of PANI–PSSMA, which is the key to maintaining its electroactivity of PANI–PSSMA in neutral solution due to the "doping effect" of the incorporated PSSMA. Therefore, PANI retains its good electroactivity during the cyclic voltammetric scan in PSSMA + $MnSO_4$ solution. The retention of electroactivity of PANI is beneficial for depositing MnO_2 in neutral solution. Fig. 1 clearly

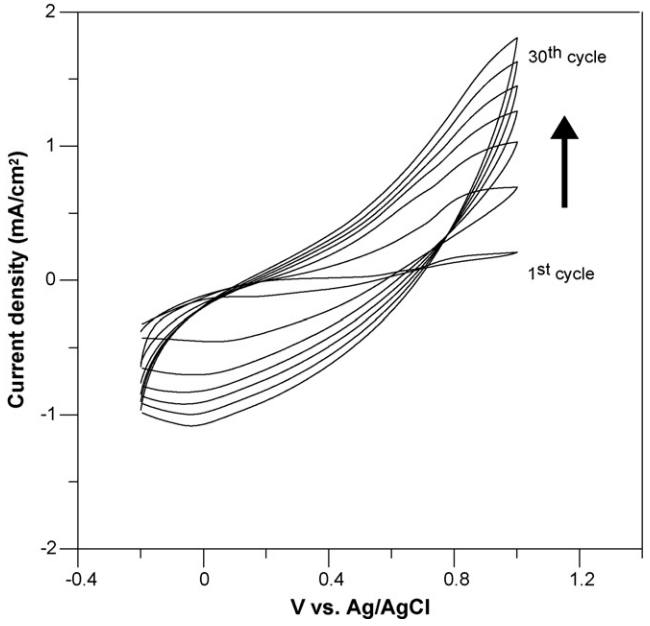

Fig. 1. Consecutive CVs of growth of MnO_2 embedded in PANI–PSSMA matrix. Cyclic voltammetry was carried out at 50 mV s^{-1} in the potential range from −0.2 to 1.0 V for 30 cycles.

shows that the anodic and cathodic currents increase with the number of cycles indicating that the anion doping of PANI accompanies the deposition of MnO_2 in PANI matrix.

Based on the observed cyclic voltammetric deposition result, a scheme for the "electrochemical doping-deposition" of MnO_2 in PANI–PSSMA matrix is proposed in Fig. 2. When $MnSO_4$ and PSSMA are mixed well, the mobile Mn^{2+} ions will couple with SO_3^- and COO^- groups on PSSMA to form a complex. During the forward scan (when a positive potential is applied), PANI emeraldine base will be doped with the excess of SO_3^- and COO^- anions on the PSSMA to maintain charge neutrality within the PANI phase. Meanwhile, the formed complex (Mn^{2+} with SO_3^- and COO^-) may become trapped in the PANI matrix during the anodic doping. As the number of deposition cycles increased, more of the complex became trapped in PANI–PSSMA accompanied by the formation of MnO_2 in the PANI–PSSMA matrix with the contribution of current increase in Fig. 1. The deposition of MnO_2 in an electrolyte that contained Mn^{2+} ions proceeds following the reaction [23]:

$$Mn^{2+} + 2H_2O \rightarrow MnO_2 + 4H^+ + 2e^- \quad (1)$$

The surface morphologies of PANI (emeraldine base) and PANI–PSSMA–MnO_2 were examined by SEM. The SEM image of PANI emeraldine base (Fig. 3a) exhibited a cauliflower-like interconnected tube structure with a large proportion of pores in a disordered arrangement. The morphology (Fig. 3b) of PANI–PSSMA–MnO_2 differed markedly from that of PANI (emeraldine base). As presented in the figure, the cauliflower-like interconnected tube structures of PANI appeared to be completely covered by spherical MnO_2 particles (in nano size). The porous PANI–PSSMA–MnO_2, which was prepared by "electrochemical doping-deposition", exhibited many nano-dimension pores and agglomerates of fine oxide particles. The prepared PANI–PSSMA–MnO_2 film had a strong ability to adhere to the substrate even without any binder. It exhibited no abruption, even when washed many times. Spherical nano-sized MnO_2 particles on PANI–PSSMA were expected to produce more sites that were susceptible to the redox reaction, increasing the active area and, consequently higher capacitance.

Fig. 4 presents the wide-angle XRD patterns of PANI and PANI–PSSMA–MnO_2. The intense XRD peaks at $2\theta = 19^\circ$ and 25° of both PANI and PANI–PSSMA–MnO_2 are similar to that of PANI in literature [24]. The additional XRD intense peak at $2\theta = 40^\circ$ is observed from PANI–PSSMA–MnO_2, indicating that the received MnO_2 is typical β-phase MnO_2 [25]. The XRD peaks of PANI–PSSMA–MnO_2 are similar to those of PANI, verifying a distortion in the crystalline structure of β-MnO_2 during the polymerization reaction, which led

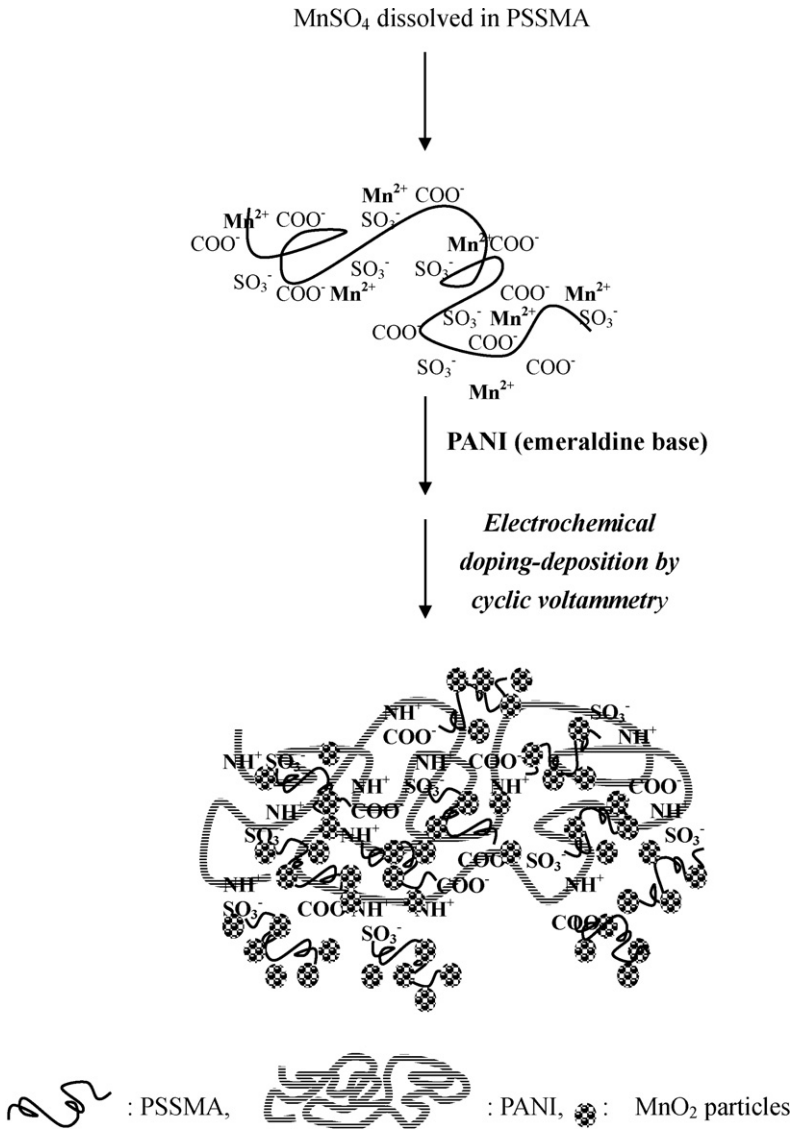

Fig. 2. Schematic illustration for the formation of PANI–PSSMA–MnO_2.

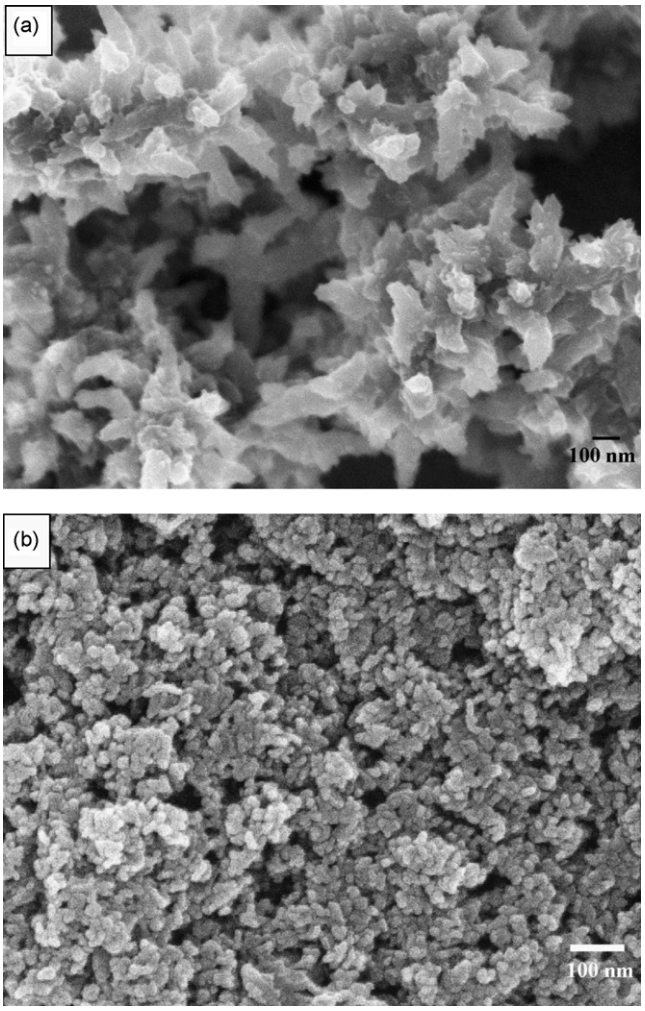

Fig. 3. SEM micrographs of (a) PANI (emeraldine base) and (b) PANI–PSSMA–MnO_2.

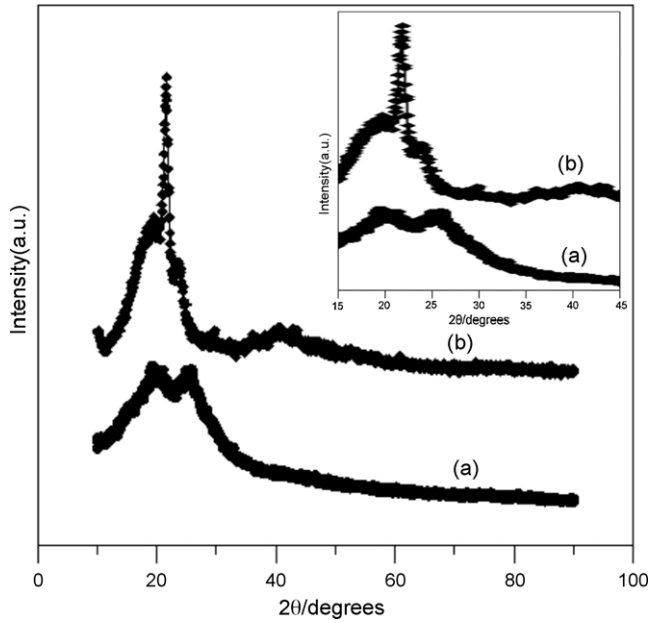

Fig. 4. X-ray diffraction patterns of (a) PANI and (b) PANI–PSSMA–MnO_2.

to the transformation of crystalline β-MnO_2 into the amorphous phase; therefore, the XRD peaks of PANI were predominant.

Fig. 5 shows the deconvoluted XPS spectra of PANI–PSSMA–MnO_2 for the signals of Mn and O elements. The survey scan (Fig. 5a) of PANI–PSSMA–MnO_2, revealing Mn 3p and Mn 2p signals, was clear evidence that MnO_2 particles had been successfully embedded in PANI–PSSMA matrix. Fig. 5a shows a broad peak of Mn $2p_{3/2}$ for PANI–PSSMA–MnO_2. The broad peak of Mn $2p_{3/2}$ indicates that PANI–PSSMA–MnO_2 comprised mixed oxy/hydrol-manganese species at various oxidation states [26]. Accordingly, the Mn $2p_{3/2}$ spectrum is consistent deconvoluted into three components (640.8, 641.9, and 642.7 eV for Mn(II), Mn(III), and Mn(IV)). Integrating the areas under the associated peaks reveals that the relative amounts of these components were 20.3%, 38.3%, and 41.4%), respectively. The observed results show that the tetravalent manganese oxide was the dominant form. Therefore, MnO_2 prepared herein in this work has a nonstoichiometric structure. This nonstoichiometric characteristic is believed to be responsible for the amorphous structure of MnO_2, plated various electrochemical modes. Fig. 5b shows the O 1s spectrum of the PANI–PSSMA–MnO_2. The spectrum can be deconvoluted into three components, which are related to the Mn–O–Mn bond (529.8 eV) for the tetravalent oxide, the Mn–OH bond (530.9 eV) for a hydrated

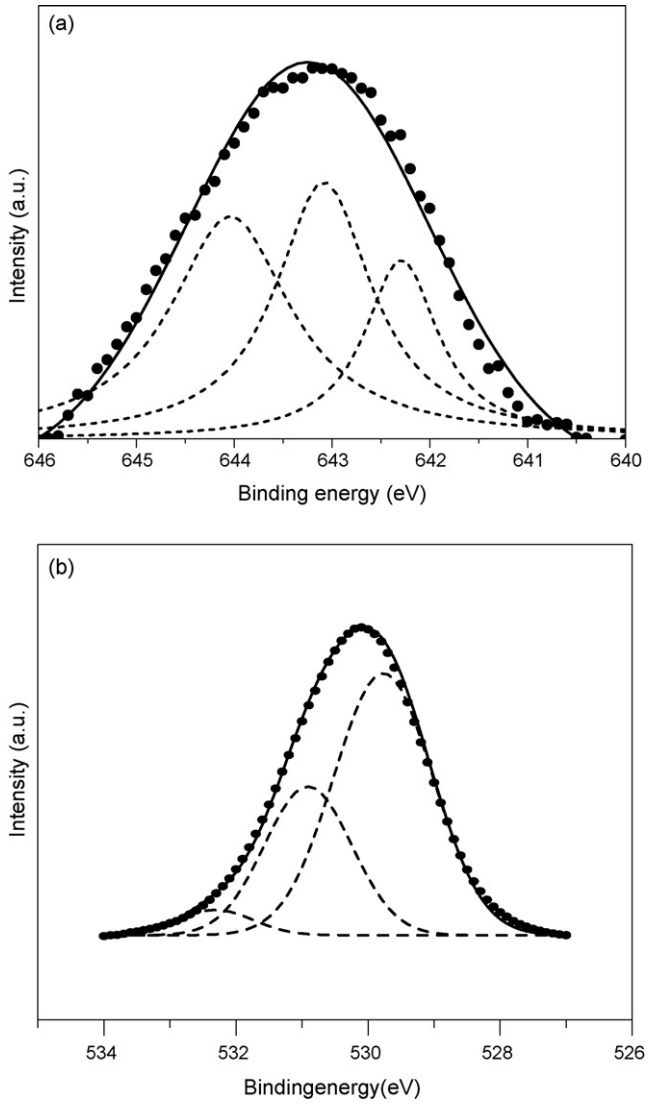

Fig. 5. XPS spectra of (a) Mn $2p_{3/2}$, and (b) O 1s for PANI–PSSMA–MnO_2.

trivalent oxide, and the H–O–H bond (532.3 eV) for residual water. Based on the relevant amounts of the three constituents for O 1s, anhydrous Mn oxide (i.e., Mn–O–Mn, 0.64) is the main species in PANI–PSSMA–MnO_2. However, a significant amount of Mn–OH (0.32) and water species (0.04) is observed in PANI–PSSMA–MnO_2, revealing the hydrous nature for MnO_2 in PANI–PSSMA. The above results show that PANI–PSSMA–MnO_2 that is prepared by "electrochemical doping-deposition" exhibits a nonstoichiometric structure with a hydrous characteristic, which is similar to that of the hydrated oxide film, prepared by electrochemical deposition [26].

3.2. Electrochemical performance

The PANI–PSSMA–MnO_2 was tested by cyclic voltammetry (CV) in a 0.5 M Na_2SO_4 solution as the electrolyte. For comparison, PANI that was prepared using APS as an oxidant was also investigated. Fig. 6 shows cyclic voltammograms of PANI and PANI–PSSMA–MnO_2, obtaining at a scan rate of 50 mV s^{-1} in a potential range of −0.2 and 1.0 V (vs. Ag/AgCl). The voltammograms clearly show that PANI–PSSMA–MnO_2 has much higher current than PANI. The enhanced current for PANI–PSSMA–MnO_2 is expected to arise from the contribution of the loading of MnO_2 nanoparticles. The specific capacitance of the electrodes is estimated using the following equation.

$$C = \frac{Q}{\Delta E m} \tag{2}$$

where C is the specific capacitance (F g^{-1}); Q is the voltammetric charge (C); ΔE is the potential window, and m is the mass of material (g).

In this work, it was found that the specific capacitance of PANI was about 18.5 F g^{-1} while the PANI–PSSMA–MnO_2 had a reasonably high specific capacitance (SC) of 50.4 F g^{-1}. After the contribution of the PANI–PSSMA host was subtracted out, the MnO_2 nanoparticles were calculated to have a high specific capacitance of about 556 F g^{-1}. PANI–PSSMA does not contribute markedly to the total capacitance of the electrode. However, its presence helps to disperse MnO_2 nanoparticles over a large area (Fig. 3b), increasing

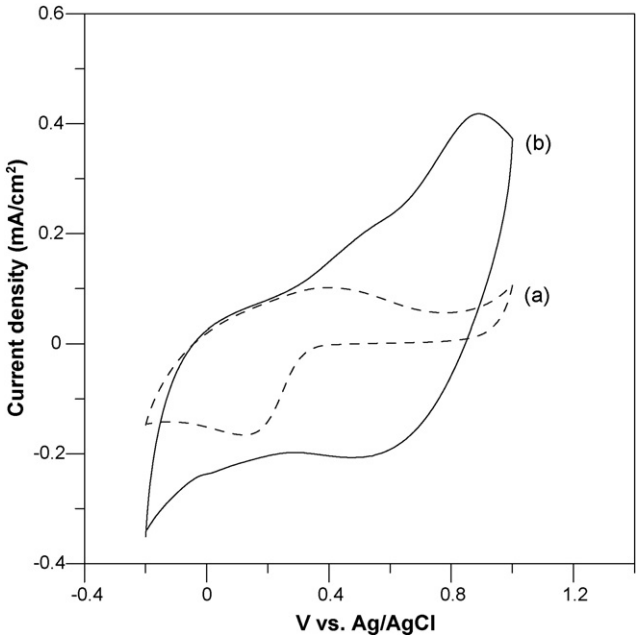

Fig. 6. Cyclic voltammograms of (a) PANI and (b) PANI–PSSMA–MnO_2 composite electrodes. Electrodes are scanned in a potential range of −0.2 to 1.0 V. The scan rate is 50 mV s^{-1}.

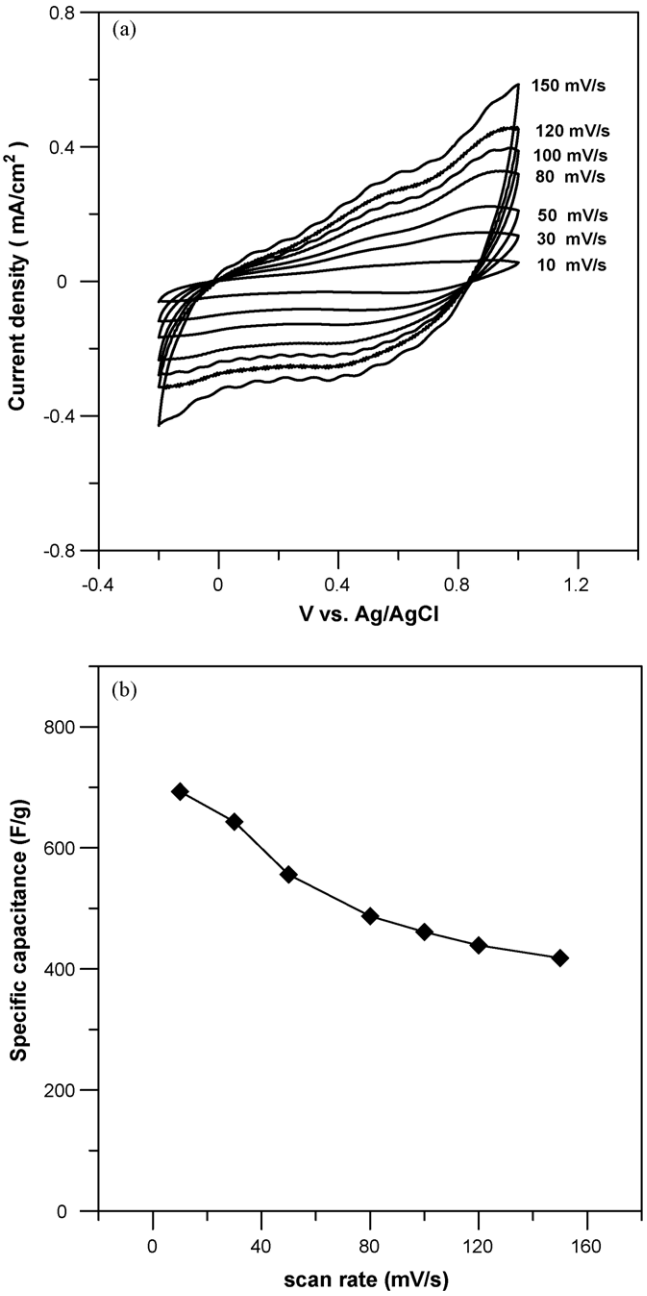

Fig. 7. (a) CVs of different scan rates and (b) effect of different potential scan rate on the specific capacitance of PANI–PSSMA–MnO_2 composite electrode.

the active surface area of MnO_2. Moreover, PANI–PSSMA is expected to act importantly as a stabilizer that prevents the aggregation of MnO_2 nanoparticles by both steric and electrostatic stabilization mechanisms. Notably, the use of conducting polymers to stabilize nanoparticles has been described elsewhere [27–29].

Fig. 7a presents the CVs at various scan rates for the PANI–PSSMA–MnO_2 in the range of −0.2 to 1.0 V in 0.5 M Na_2SO_4 solution. The CV curves increase with increasing the scan rate and I–E responses showing oxidation and reduction bipolar symmetry [30], indicating that Faraday redox reactions are highly electrochemically reversible. Fig. 7b plots the variation of the specific capacitance value with the scan rate of CV for the PANI–PSSMA–MnO_2. The maximum SC value of 693 was obtained at a CV scan rate of 10 mV s^{-1} with the PANI–PSSMA–MnO_2. Interestingly, a SC value of 418 was obtained even at a high CV scan rate of 150 mV s^{-1}, indicating the high power density of

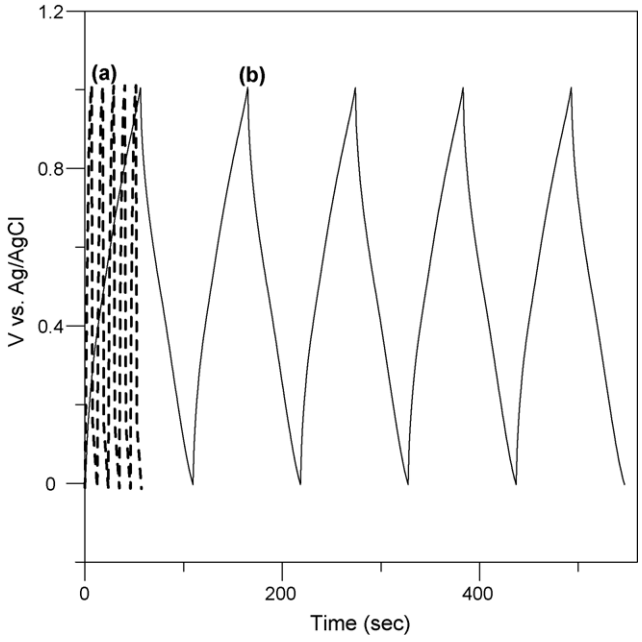

Fig. 8. Galvanstatic charge–discharge cycling in 0.5 M Na_2SO_4 for the (a) PANI and (b) PANI–PSSMA–MnO_2 electrodes.

the PANI–PSSMA–MnO_2. These values for PANI–PSSMA–MnO_2 are higher than those in the literature [19,12,31,32] for various MnO_2 composite electrodes. The formation of nanostructured and microporous materials was attributed to the high values of electrical parameter in this work. The "electrochemical doping-deposition" method of synthesis and the materials used herein are commercially and econometrically favorable.

Fig. 8 plots the charge–discharge behavior of PANI and PANI–PSSMA–MnO_2 electrodes. The typical result was measured from 0.0 to 1.0 V versus Ag/AgCl in 0.5 M Na_2SO_4 at the current density of 100 $\mu A\,cm^{-2}$. As shown in Fig. 8, the charge curve is highly symmetric with the corresponding discharge counterparts over the entire potential region of the PANI–PSSMA–MnO_2 electrode. The area under the charge–discharge clearly increased when MnO_2 nanoparticles incorporated into the PANI–PSSMA matrix (curve b). The observed results are consistent with the cyclic voltammograms in Fig. 6. The SC is calculated form the charge–discharge curves by the following equation:

$$C = \frac{i \times t}{m \times \Delta V} \tag{3}$$

The SC values C for the PANI and PANI–PSSMA–MnO_2 electrodes calculated from Eq. (3) were 17.8 and 49.7 $F\,g^{-1}$, respectively, which are close to the SC values of 18.5 and 50.4 $F\,g^{-1}$ obtained from the CV. The obvious enhancement in the capacitance of PANI–PSSMA–MnO_2 is attributed to the uniform dispersion of MnO_2 nanoparticles in the PANI–PSSMA matrix. The dispersion of MnO_2 nanoparticles in the PANI–PSSMA matrix increases the utilization of MnO_2 nanoparticles, markedly increasing the specific capacitance of this composite material. Additionally, PANI--PSSMA has a dual route by providing an efficient route for the shuttling of electronic charges to deliver the proton as well as promoting the adhesion of MnO_2 nanoparticles to the current collector to reduce the contact resistance.

4. Conclusion

This work elucidates a new method for simultaneously doping PANI with polyelectrolyte (PSSMA) and depositing MnO_2 nanoparticles in the conducting polymer matrix. SEM images revealed that MnO_2 nanoparticles were highly dispersed in the PANI–PSSMA porous structure. XRD and XPS provide evidences that the composite consists of PANI–PSSMA and β-MnO_2 nanoparticles. The PANI–PSSMA–MnO_2 composite has a greater specific capacitance (556 $F\,g^{-1}$ for MnO_2) than PANI and MnO_2 in 0.5 M Na_2SO_4 solution. The strategy for constructing nanocomposite electrode material can be extended to other conductive polymers and inorganic metal oxides such as polypyrrole, polythiophene, and ruthenium oxide.

Acknowledgements

The authors wish to thank the National Science Council in Taiwan for financial support of this work (grant number NSC 94-2622-E-239-012-CC).

References

[1] B.E. Conway, J. Electrochem. Soc. 138 (1991) 1539.
[2] Q.H. Huang, X.Y. Wang, J. Li, Electrochim. Acta 52 (2006) 1758.
[3] J.H. Jang, K. Machida, Y. Kim, K. Naoi, Electrochim. Acta 52 (2006) 1733.
[4] L.M. Huang, H.Z. Lin, T.C. Wen, A. Gopalan, Electrochim. Acta 52 (2006) 1058.
[5] C.C. Hu, T.W. Tsou, Electrochim. Acta 47 (2002) 3523.
[6] J.N. Broughton, M.J. Brett, Electrochim. Acta 50 (2005) 4814.
[7] E.R. Pinero, V.E. Khomenko, F.E. Beguin, J. Electrochem. Soc. 152 (2005) A229.
[8] K.R. Prasad, N. Miura, J. Power Sources 135 (2004) 354.
[9] K.R. Prasad, N. Miura, Electrochem. Commun. 6 (2004) 1004.
[10] M. Toupin, T. Brousse, D. Belanger, Chem. Mater. 16 (2004) 3184.
[11] K.H. An, K.K. Jeon, J.K. Heo, S.C. Lim, D.J. Bae, Y.H. Lee, J. Electrochem. Soc. 149 (2002) A1058.
[12] Z. Zhou, N. Cai, Y. Zhou, Mater. Chem. Phys. 94 (2005) 371.
[13] P. Soudan, J. Gaudet, D. Guay, D. Be langer, R. Schulz, Chem. Mater. 14 (2002) 1210.
[14] J.W. Long, A.L. Yound, D.R. Rolison, J. Electrochem. Soc. 150 (2003) A1161.
[15] R.N. Reddy, R.G. Reddy, J. Power Sources 124 (2003) 330.
[16] C.C. Hu, T.W. Tsou, Electrochem. Commun. 4 (2002) 105.
[17] C.C. Hu, C.C. Wang, J. Electrochem. Soc. 150 (2003) A1079.
[18] B. Djurfors, J.N. Broughton, M.J. Brett, D.G. Ivey, J. Electrochem. Soc. 153 (2006) A64.
[19] E.C. Rios, A.V. Rosario, R.M.Q. Mello, L. Micaroni, J. Power Sources 163 (2007) 1137.
[20] X. Zhang, L.Y. Ji, S.C. Zhang, W.S. Yang, J. Power Sources 173 (2007) 1017.
[21] M. Pourbaix, Atlas of Electrochemical Equilibria in Aqueous Solutions, National Association of Corrosion Engineers, Houston, Texas, USA, 1966.
[22] T.C. Wen, L.M. Huang, A. Gopalan, Electrochim. Acta 46 (2001) 2463.
[23] S. Rodrigues, N. Munichandraiah, A.K. Shukla, J. Appl. Electrochem. 28 (1998) 1235.
[24] J.P. Pouget, M.E. Jo'zefowicz, A.J. Epstein, X. Tang, A.G. MacDiarmid, Macromolecules 24 (1991) 779.
[25] A.H. Gemeay, I.A. Mansour, R.G. El-Sharkawy, A.B. Zaki, Eur. Polym. J. 41 (2005) 2575.
[26] J.K. Chang, W.T. Tsai, J. Electrochem. Soc. 150 (2003) A1333.
[27] A.Z. Ernst, S. Zoladek, K. Wiaderek, J.A. Cox, A. Kolary-Zurowska, K. Mieunikowski, P.J. Kulesza, Electrochim. Acta 53 (2008) 3924.
[28] A. Mourato, J.P. Correia, H. Siegenthaler, L.M. Abrantes, Electrochim. Acta 53 (2007) 664.
[29] C. Jiang, X.Q. Lin, J. Power Sources 164 (2007) 49.
[30] N. Nagarajan, H. Humadi, I. Zhitomirsky, Electrochim. Acta 51 (2006) 3039.
[31] J. Li, X. Wang, Q.H. Huang, S. Gamboa, P.J. Sebastian, J. Power Sources 160 (2006) 1501.
[32] T. Xue, C.L. Xu, D.D. Zhao, X.H. Li, H.L. Li, J. Power Sources 164 (2007) 953.